PHYSICAL REVIEW B VOLUME 43, NUMBER 10 1 APRIL 1991

Diffraction from random alloys

M. F. Thorpe, J. S. Chung,* and Y. Cai
Department of Physics and Astronomy and Center for Fundamental Materials Research, Michigan State University, East Lansing, Michigan 48824
(Received 12 September 1990)

We calculate the diffraction from a random alloy, consisting of bonds of different natural lengths. The resulting structure is a distorted crystal with strong correlations between displacements at different sites. The diffraction pattern is dominated by a set of Bragg peaks whose intensity is modulated by a Debye-Waller factor. At the base of each of these Bragg peaks, we find divergent Huang scattering due to the second-order correlations between displacements. Higher-order correlations produce a negligible nondivergent background. Results are obtained in closed form and compared with computer simulations.

I. INTRODUCTION

The elastic scattering (diffraction) from a random alloy is a complex problem that has received considerable attention over the years. In this paper, we describe the diffraction pattern caused by the correlated static displacements from an underlying crystalline structure. We find a set of Bragg peaks (determined by the average lattice), modified by an appropriate Debye-Waller factor. Each Bragg peak has some diffuse (Huang) scattering associated with it. To quote from Huang,[1] "Considering a crystal lattice formed of randomly distributed atoms of two kinds mixed in comparable proportions, it must obviously be extremely difficult to describe qualitatively the distorted configuration," and he goes on to consider the case of isolated impurities. Modern analytic techniques and computer simulations now allow us to treat the concentrated alloy. Although the example worked through here is simple, we have found it instructive and we hope the reader will too.

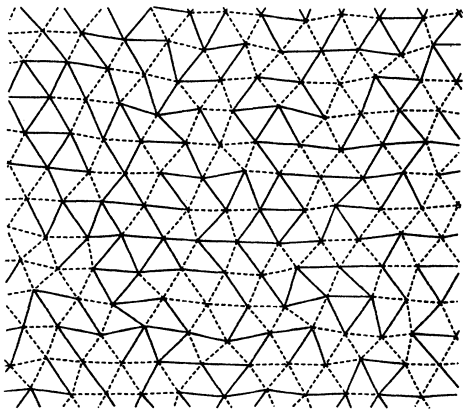

FIG. 1. A piece of a relaxed random triangular network. This figure is reproduced from I. The short bonds are shown as dashes and the long bonds by solid lines. The sample shown has equal numbers of short and long bonds ($x=0.5$) and the natural length of the long bonds is 30% greater than the natural length of the short bonds. The two spring constants are equal.

We use the model alloy of Thorpe and Garboczi[2] (henceforth referred to as I) for an $A_{1-x}B_x$ alloy. This consists of a crystalline lattice containing two kinds of *bonds*, A and B which are randomly positioned throughout the lattice with probabilities $1-x$ and x, respectively. The static structure is obtained by minimizing the energy associated with the potential

$$V=\frac{K}{2}\sum_{\langle ij\rangle}(|\mathbf{R}_i-\mathbf{R}_j|-L_{ij}^0)^2 . \tag{1}$$

Here L_{ij}^0 can take on the values L_A^0 and L_B^0 with probability $1-x$ and x, respectively. The summation goes over all nearest-neighbor bonds ij and the angular brackets denote that nearest-neighbor bonds are only counted once. The vector $\mathbf{R}_i$ goes to the site i at the end of the bond ij from some (arbitrary) origin. The potential (1) can be minimized with respect to the $\mathbf{R}_i$ to give

$$O=\sum_j[(\mathbf{R}_i-\mathbf{R}_j)-L_{ij}^0\hat{\mathbf{R}}_{ij}] . \tag{2}$$

Here $\hat{\mathbf{R}}_{ij}$ is a unit vector along the relaxed bond direction. These equations determine the equilibrium positions of all the sites, as described fully in I. An example is shown in Fig. 1, which can be visualized as static concentration waves of all wavelengths freezing out from a perfect crystalline lattice. We will take all the spring constants to be equal in this paper as it simplifies the analytic treatment as discussed in I, and does not qualitatively effect the result.

II. COMPUTER SIMULATIONS

We have used a fcc lattice rather than the triangular net as in I. This is because of the well-known instability of two-dimensional lattice ordering to fluctuations.[3] While this does not effect quantities like the mean bond length, it does have a profound effect on the diffraction pattern, which is very sensitive to long-range order. The

general formalism of I, which is geared towards the calculation of local distances, applies equally well in any dimension. We have used $M\times M\times M$ fcc samples (with $M=20$) and periodic boundary conditions containing $N=4M^3=32\,000$ atoms and $24M^3=192\,000$ bonds, which were randomly assigned to be A or B with probability $1-x$ or x, respectively. The simulation program, which uses a variant of the conjugate gradient method,[4] adjusted the positions of all the atoms *and* the size of the supercell to minimize the energy. The simulation was terminated when the energy agreed with the exact energy $3Nx(1-x)(L_B^0-L_A^0)^2/2$ as given in I, to better than 1%. All other quantities, in particular, mean lengths and fluctuations in the lengths, agreed with the exact results in I to better than a percent, so that we had confidence that the samples were fully relaxed. The supercell was kept strictly cubic to facilitate the analysis. The mean bond length $\langle L\rangle$, which is proportional to the sample size, is given by Vegard's law as discussed in I,

$$\langle L\rangle=(1-x)L_A^0+xL_B^0\ . \tag{3}$$

The diffraction pattern was computed from the relaxed coordinates using

$$I(\mathbf{Q})=\frac{1}{N}\left|\sum_i \exp(i\mathbf{Q}\cdot\mathbf{R}_i)\right|^2\ , \tag{4}$$

where $I(Q)$ is the scattered intensity per site, and Q is the scattering vector.

A. Bragg scattering

The diffraction pattern is dominated by the Bragg peaks shown in Fig. 2 for different directions in reciprocal space and for different values of the length mismatch parameter $(L_B^0-L_A^0)/\bar{L}$. The Bragg peaks are Kronecker δ functions, rather than Dirac δ functions, because of the finite size of the supercell. We have taken out a factor N from the computed intensity to make the connection between the computed Kronecker δ functions and the calculated Dirac δ functions, used in the next section. These Bragg peaks have no width and are associated with a single superlattice point in reciprocal space. It can be seen that the diffracted intensity falls off as a Gaussian in all three cubic directions. This is certainly what would be naively expected, and is similar to the situation with dynamic disorder caused by phonons that produces a Debye-Waller factor.[5]

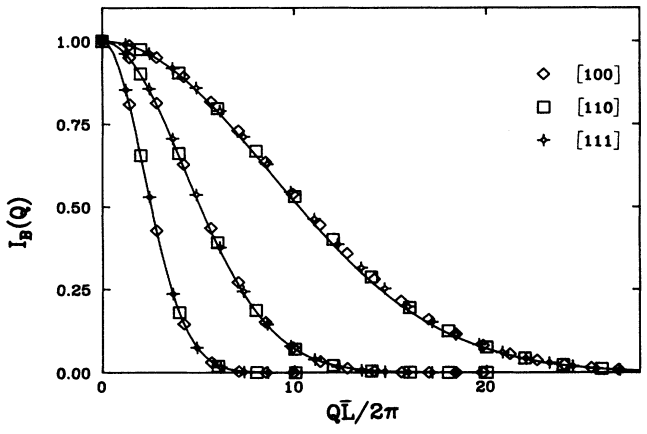

FIG. 2. The Bragg scattering for a random fcc alloy with two kinds of bond lengths, similar to that shown in Fig. 1. The length mismatch parameters are 4% (upper curve), 8% (middle curve), and 16% (lower curve) and the concentration $x=0.5$. The symbols indicate the different cubic directions and the solid line is the Debye-Waller factor calculated in the text. The intensity is averaged over the different equivalent directions of a single sample. The solid line is the theory (8) using the Debye-Waller factor (12).

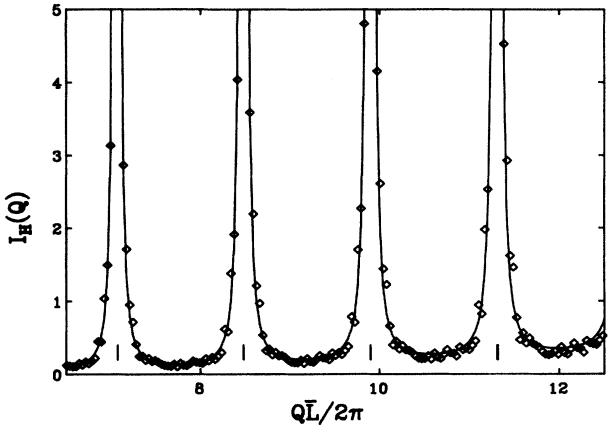

FIG. 3. The Huang scattering in the 100 direction for a random fcc alloy with two kinds of bond lengths. The length mismatch parameter is 4% and the concentration $x=0.5$. This figure is a magnified version of the Bragg peaks shown in Fig. 2 and is averaged over the different [100] directions for nine samples. The solid line is the theory (16) given in the text and the vertical bars mark the positions of the Bragg peaks shown in Fig. 2.

B. Huang scattering

The computed background is artificially reduced by a factor N with respect to the Bragg peaks because of the

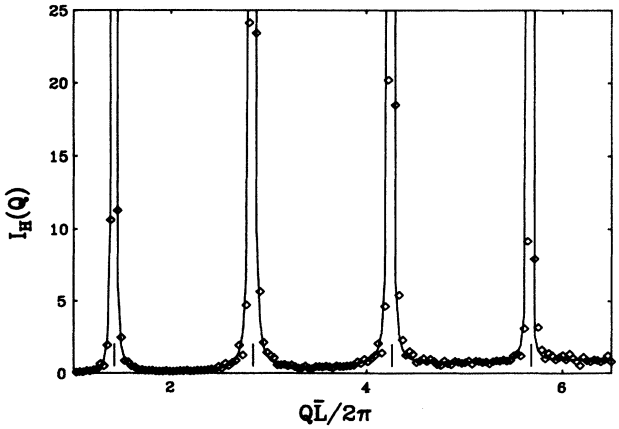

FIG. 4. The same as Fig. 3, except that the lattice mismatch parameter has been increased to 16%.

Kronecker δ functions caused by the supercell, and therefore cannot be seen in Fig. 2. The background scattering is shown in Figs. 3 and 4 for different values of the length mismatch parameter. The noise in the results was greater than for the Bragg peaks and so we have averaged over nine samples. The scattering intensity is shown at the $2M-1=39$ superlattice points between pairs of Bragg peaks in the [100] direction. This Huang scattering[1] is seen to be largest in the vicinity of the Bragg peaks in the [100] direction. Similar results are found around all the Bragg peaks.

III. THEORY

It is convenient to separate the scattering into two parts: the Bragg scattering $I_B(\mathbf{Q})$, and the remainder that we will refer to as the Huang scattering $I_H(\mathbf{Q})$, so that

$$I(\mathbf{Q})=I_B(\mathbf{Q})+I_H(\mathbf{Q}) . \tag{5}$$

A. Bragg scattering

The cross section (4) can be conveniently rewritten as

$$I(\mathbf{Q})=\frac{1}{N}\sum_{i,j}\exp[i\mathbf{Q}\cdot(\mathbf{R}_i^0-\mathbf{R}_j^0)]\langle\exp[i\mathbf{Q}\cdot(\mathbf{u}_i-\mathbf{u}_j)]\rangle , \tag{6}$$

where $\mathbf{R}_i=\mathbf{R}_i^0+\mathbf{u}_i$, and the $\mathbf{R}_i^0$ define the underlying mean lattice and the $\mathbf{u}_i$ represent the (small) displacements from it. The angular brackets $\langle\cdots\rangle$ in (6) denote an ensemble average over different static configurations. The size of the mean lattice is given by Vegard's law (3). Inasmuch as the diffraction pattern is dominated by the Bragg peaks as shown in Fig. 2, it is suggestive that we should make the conventional approximation[5]

$$\langle\exp[i\mathbf{Q}\cdot(\mathbf{u}_i-\mathbf{u}_j)]\rangle\approx\langle\exp(i\mathbf{Q}\cdot\mathbf{u}_i)\rangle\langle\exp(-i\mathbf{Q}\cdot\mathbf{u}_j)\rangle$$
$$=\exp(-2W), \tag{7}$$

which assumes that the displacements at each site are independent, as with "frozen Einstein oscillators," where the displacement at each site is chosen independently. This is manifestly not the case here, as we will discuss later. Nevertheless, the assumption (7) leads to excellent answers. Inserting (7) into (6), we find that

$$I_B(\mathbf{Q})=\exp(-2W)\delta(\mathbf{Q}-\mathbf{g}), \tag{8}$$

where $\mathbf{g}=(\sqrt{2}\pi/\bar{L})(n_1,n_2,n_3)$ with the integers n_1,n_2,n_3 either all even or all odd, are the reciprocal-lattice vectors for the fcc lattice with a mean lattice spacing $\bar{L}$ given by Vegard's law (3).

In I, it was shown that the displacements $\mathbf{u}_i$ could be expanded in terms of the Green functions $\overleftrightarrow{G}_{ij}$ of the perfect lattice, the various natural bond lengths L_{ij}^0, and the nearest-neighbor vector directions $\hat{\mathbf{R}}_{ij}$ of the perfect lattice

$$\mathbf{u}_i=K\sum_{l,m}\overleftrightarrow{G}_{il}\cdot\hat{\mathbf{R}}_{lm}(L_{lm}^0-\langle L\rangle) . \tag{9}$$

After some manipulation, of the kind discussed in I, and involving doing the statistical averaging[6] over the (random) bonds, we may write the *full* Debye-Waller factor as

$$W=-\tfrac{1}{2}\sum_{l,m}\ln\{1-4x(1-x)\sin^2[\tfrac{1}{2}K\mathbf{Q}\cdot\overleftrightarrow{G}_{il}\cdot\hat{\mathbf{R}}_{lm}(L_B^0-L_A^0)]\} . \tag{10}$$

For reasonable values of the length mismatch parameter $(L_B^0-L_A^0)/\bar{L}$, the argument of the sine term in (10) is small and so, to leading order,

$$W=\tfrac{1}{2}K^2x(1-x)(L_B^0-L_A^0)^2\sum_{l,m}(\mathbf{Q}\cdot\overleftrightarrow{G}_{il}\cdot\hat{\mathbf{R}}_{lm})^2$$
$$=\tfrac{1}{2}\langle(\mathbf{Q}\cdot\mathbf{u})^2\rangle=\frac{Q^2}{6}\langle u^2\rangle , \tag{11}$$

which is the *conventional* Debye-Waller factor. We have dropped the site label from $\langle u^2\rangle$ since it is the same for all sites. After some manipulation, we find the result,

$$W=\frac{Q^2}{6}\langle u^2\rangle=\frac{K}{2}Q^2x(1-x)(L_B^0-L_A^0)^2\langle 1/\omega^2\rangle , \tag{12}$$

where $\langle 1/\omega^2\rangle$ is the mean inverse squared frequency of the fcc lattice with nearest-neighbor springs K. The "phonon" band[7] is defined by the frequencies $0<\omega^2<8$ K, and we find, by numerical integration, that $\langle 1/\omega^2\rangle^{-1}=2.38$ K.

B. Huang scattering

By subtracting the Bragg scattering (8) from the total scattering (4), we find the Huang scattering[1,8,9] is given by

$$I_H(\mathbf{Q})=\exp(-2W)\times\frac{1}{N}\sum_{i,j}\exp[i\mathbf{Q}\cdot(\mathbf{R}_i^0-\mathbf{R}_j^0)]\times\{\langle\exp[i\mathbf{Q}\cdot(\mathbf{u}_i-\mathbf{u}_j)]\rangle\exp(2W)-1\} \tag{13}$$

This is as hard as the original expression to evaluate, and so we approximate (13) by expanding the terms in the final square bracket. The approximation (7) is replaced by the improved approximation

$$\langle \exp[i\mathbf{Q}\cdot(\mathbf{u}_i-\mathbf{u}_j)]\rangle = \begin{cases} \exp(-2W)[1+\langle(\mathbf{Q}\cdot\mathbf{u}_i)(\mathbf{Q}\cdot\mathbf{u}_j)\rangle+O(Q^4)] & \text{for } i\neq j, \\ 1 \quad \text{for } i=j\ . \end{cases} \tag{14}$$

Note that, because of inversion symmetry, the correction terms to (14) are $O(Q^4)$. Doing the summations, we are led to the result[6]

$$\begin{aligned} I_H(\mathbf{Q}) &\approx 1-(1+2W)\exp(-2W)+\exp(-2W)\frac{1}{N}\sum_{i,j}\exp[i\mathbf{Q}\cdot(\mathbf{R}_i^0-\mathbf{R}_j^0)]\langle(\mathbf{Q}\cdot\mathbf{u}_i)(\mathbf{Q}\cdot\mathbf{u}_j)\rangle \\ &= 1-(1+2W)\exp(-2W)+\exp(-2W)\langle(\mathbf{Q}\cdot\mathbf{u}_q)(\mathbf{Q}\cdot\mathbf{u}_{-q})\rangle \\ &= [1-(1+2W)\exp(-2W)]-\exp(-2W)Kx(1-x)(L_B^0-L_A^0)^2\mathbf{Q}\cdot\overleftrightarrow{G}(\mathbf{q})\cdot\mathbf{Q}\ . \end{aligned} \tag{15}$$

Here $\mathbf{u}_q$ is the Fourier transform of the displacements $\mathbf{u}_i$, and $\mathbf{q}=\mathbf{Q}-\mathbf{g}$ is the reduced scattering vector that is measured from the nearest Bragg point. The Green function $\overleftrightarrow{G}(\mathbf{q})$ is periodic in reciprocal space and is the Fourier transform of $\overleftrightarrow{G}_{ij}$, which diverges at small q as q^{-2}. The term

$$[1-(1+2W)\exp-(2W)]$$

in (15) is small and accounts for most of the background away from the Bragg peaks. For this reason, it is important to include the higher-order *diagonal* terms, even though the higher-order *off-diagonal* terms are neglected in (14). The last term in expression (15) does not lead to large scattering near the origin because the q^{-2} divergence is cancelled by the Q^2 factor in (15). However, this divergence remains at all Bragg peaks. Note that this divergence is integrable because of the phase-space factor in three dimensions. We have lumped together all the non-Bragg terms into (15) for convenience, although they could have been separated into a diffuse background term (the first term in square brackets) and the divergent scattering (last term). The result (15) along the principal cubic directions becomes

$$I_H(\mathbf{Q})=1-(1+2W)\exp(-2W)+\tfrac{1}{8}\exp(-2W)x(1-x)[Q(L_B^0-L_A^0)]^2/\sin^2\phi\ , \tag{16}$$

where $\phi=q\bar{L}/\sqrt{8}$ in the [100] direction and $\phi=q\bar{L}/\sqrt{6}$ in the [111] direction. The divergences in (16) occur at the Bragg peaks ($\phi=n\pi$, where n is any nonzero integer). We show the results along the [100] direction in Figs. 3 and 4 for different values of the length mismatch parameter $(L_B^0-L_A^0)/\bar{L}$. Although the Huang scattering falls away from the Bragg peak as q^{-2} in all directions, it is not isotropic around the Bragg peak as can be seen from (15). In some directions, as in Figs. 3 and 4, the coupling is entirely to the longitudinal phonon modes, while in others it is entirely to the transverse modes. This is different from the scattering from single isolated site impurities[8] where the spherically symmetric strain field leads to only a longitudinal coupling. The difference arises because we are alloying bonds and not sites in our model system.

To estimate the total integrated strength, we make the rough assumption that the scattering is isotropic around each Bragg peak, and integrate the last term in (16) inside a sphere of radius equal to half the spacing to the nearest Bragg peak in the same principal direction. This leads to the ratio of intensities

$$I_H(g)/I_B(g)=Ax(1-x)[g(L_B^0-L_A^0)]^2\ , \tag{17}$$

where A is a constant that is ~ 0.1. This is to be expected from sum-rule considerations. If the length mismatch parameter $(L_B^0-L_A^0)/\bar{L}$ is increased slowly from zero, then the intensity of a Bragg peak is decreased by a factor $\exp(-2W)\approx 1-2W$, and the intensity

$$\begin{aligned} 2W &= x(1-x)[g(L_B^0-L_A^0)]^2K\langle 1/\omega^2\rangle \\ &= 0.42x(1-x)[g(L_B^0-L_A^0)]^2 \end{aligned}$$

appears at the base of the Bragg peak as the Huang scattering. These estimates are in agreement apart from a numerical factor of about 4, due to the rough integration that was done to obtain (17). Note that the background term $1-(1+2W)\exp(-2W)$ in (16) is $O(Q^4)$. The Q dependence of the Huang scattering $g^2\exp(-\langle u^2\rangle g^2/3)$ means that it is absolute maximum at $g^2=3/\langle u^2\rangle$ when the Debye-Waller factor is down by a factor $e^{-1}=0.368$. However, relative to the Bragg peak, the Huang scattering keeps on increasing in intensity as Q increases as given in (15).

The q^{-2} divergence of the Huang scattering at the Bragg peaks is due entirely to the correlations between the displacements $\mathbf{u}_i$. When the displacements at each site are independent, as with "frozen Einstein oscillators," the expression (14) leads to an intensity $1-\exp(-2W)$ for the Huang scattering which is just a nondivergent background.

IV. RESULTS

To make a direct check of the result (12), we have obtained $\langle u^2\rangle$ from the simulation results. To do this it was necessary to superimpose and position a perfect fcc grid of the appropriate size as given by (3). The positioning was done by minimizing $\sum_i u_i^2$ with respect to rigid

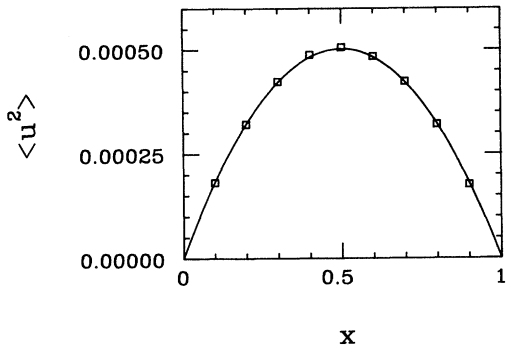

FIG. 5. Illustrating the parabolic dependence of the mean-squared displacement $\langle u^2 \rangle$ for a random fcc alloy as a function of the composition. The squares are from the computer simulation and the solid line is the theoretical result (12). The natural bond lengths are 0.98 and 1.02, so that the length mismatch parameter is 4%.

motions of the grid to obtain the best registry. The results are shown in Fig. 5, where the agreement with the parabolic composition dependence $x(1-x)$ and overall magnitude of $\langle u^2 \rangle$ is verified. Note that there are no adjustable parameters in (12), as we have calculated the magnitude via the inverse second-frequency moment of the fcc lattice.

A. Bragg scattering

We show result (8) for the Bragg scattering $I_B(\mathbf{Q})$ in Figs. 2 and 6, where the Debye-Waller factor is obtained from (12). The agreement, involving a total more than 50 separate Bragg peaks, is very good. Some simulation points lie slightly above the theoretical Debye-Waller factor, especially at intermediate Q values for a 4% mismatch. This small discrepancy at intermediate Q may be real and due to higher-order terms in Q^2 in the full Debye-Waller factor as written in (10). We note that we have no higher-order anharmonic terms in our potential

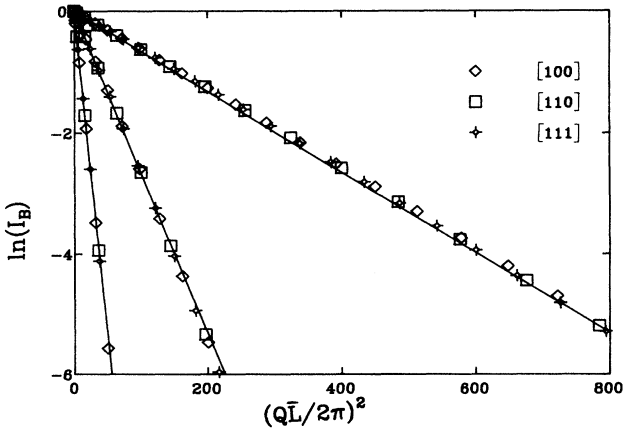

FIG. 6. The same as Fig. 2, but shown as the logarithm of the Bragg intensities plotted against the square of the wave vector. This is referred to as a Wilson plot when used to analyze experimental data (Ref. 10).

(1) which would also modify the Debye-Waller factor.[11] We have computed the displacement-displacement correlation function for nearest-neighbor sites with the result[12] that $\langle \mathbf{u}_i \cdot \mathbf{u}_j \rangle / \langle u^2 \rangle = 0.08$ and

$$3\langle (\mathbf{u}_i \cdot \hat{\mathbf{R}}_{ij})(\mathbf{u}_j \cdot \hat{\mathbf{R}}_{ij}) \rangle / \langle u^2 \rangle = 0.40 \ .$$

While these correlations fall off rapidly with distance, in no sense are the local displacements associated with the static concentration wave uncorrelated. Our results show that these correlations have no effect on the Bragg scattering.

B. Huang scattering

We show the result (16) for the Huang scattering $I_H(\mathbf{Q})$ in Figs. 3 and 4 for two different values of the lattice mismatch parameter. It can be seen that the agreement between theory and the simulation results is very good, especially considering that the approximation (14) has been made in the theory. The fit is equally good at all Q values, except that, at large Q, the scattering is weak due to the Debye-Waller factor (see Fig. 2) and the simulations become noisy. This result pleasantly surprised us because the approximation (14) is only good to $O(Q^2)$ in the off-diagonal terms. It appears that the higher-order off-diagonal terms are insignificant and nondivergent.

There is no evidence for any rounding of the peak, as would occur if the q^{-2} divergence were associated with the wings of a Lorentzian. Equally, there is also no evidence for additional divergent terms as might have occurred from the higher-order terms ignored in the approximation (14). It might have been expected that differences would appear when the lattice mismatch parameter was as large as 16%, but the comparison between theory and simulation is about as good in Fig. 4 as in Fig. 3. In effect, there is a conspiracy so that, when $[g(L_B^0 - L_A^0)]^2$ is large, the scattering is weak due to the Debye-Waller factor.,

V. DISCUSSION

As well as the static effects considered here, the thermal vibrations about the distorted static lattice, such as shown in Fig. 1, also contribute to the observed scattering. The cross section in (6) is modified to give

$$I(\mathbf{Q}) = \frac{1}{N} \sum_{i,j} \exp[i\mathbf{Q}\cdot(\mathbf{R}_i^0 - \mathbf{R}_j^0)] \langle \exp[i\mathbf{Q}\cdot(\mathbf{u}_i - \mathbf{u}_j)] \rangle \times \langle \exp[i\mathbf{Q}\cdot(\mathbf{u}_i^T - \mathbf{u}_j^T)] \rangle_T \ , \quad (18)$$

where $\mathbf{R}_i = \mathbf{R}_i^0 + \mathbf{u}_i + \mathbf{u}_i^T$ and the $\mathbf{u}_i^T$ are the *thermal* displacements. The thermal average[13] $\langle \cdots \rangle_T$ is independent of the static average, when both the static and dynamic displacements are controlled by the potential (1). The approximation (7), when applied to the expression (18), means that the total Debye-Waller factor is a product of the static part discussed previously, and a thermal part which has the form[13] $\exp(-2W_T)$ so that

$$W \rightarrow W + W_T \ ,$$

where

$$W_T=\frac{Q^2}{6}\langle (u^T)^2\rangle_T=\frac{\hbar Q^2}{2M}\langle [n(\omega)+\tfrac{1}{2}]/\omega\rangle \tag{19}$$

and $n(\omega)=[\exp(\hbar\omega/k_BT)+1]^{-1}$ is the Planck function. All the expressions in the previous sections must be modified using the replacement (19). At low temperatures the thermal part of (19) involves only the zero-point vibrations, which are small except for very light atoms. At high temperatures (greater than the Debye temperature), we obtain the classical result

$$W_T=\frac{k_BT}{2M}\langle 1/\omega^2\rangle \ . \tag{20}$$

This is the same $\langle 1/\omega^2\rangle$ that occurs in the static Debye-Waller factor (12), except that the mass M is relevant. For the static distortions, the mass was irrelevant and set equal to 1. For the fcc lattice, the phonon band is now defined by $0<\omega^2<8K/M$ so that the thermal Debye-Waller factor (20) is larger than the static Debye-Waller factor (12) if

$$k_BT>x(1-x)K(L_B^0-L_A^0)^2 \ , \tag{21}$$

which compares the thermal energy k_BT to the potential energy associated with a displacement $L_B^0-L_A^0$, weighted with the usual alloy factor $x(1-x)$. We note from I that the strain energy/per bond

$$\varepsilon=Kx(1-x)(L_B^0-L_A^0)^2/4$$

so that (21) is equivalent to $k_BT>4\varepsilon$. The condition (21) is quite general and not lattice specific as all the lattice effects occur through the common factor $\langle 1/\omega^2\rangle$.

In thermal neutron scattering, the neutron has a low energy so that the "transit time" for the neutron is sufficiently long that it sees the time-averaged lattice. The phonon motion leads to Bragg scattering modified by a Debye-Waller factor $\exp[-2(W+W_T)]$, as discussed in the previous paragraph. The term involving $\langle(\mathbf{Q}\cdot\mathbf{u}_i^T)(\mathbf{Q}\cdot\mathbf{u}_j^T)\rangle_T$ that arises when (18) is subject to the approximation (14), leads to one-phonon *inelastic* scattering. Thus, there is no thermal equivalent of Huang scattering and all the elastic q^{-2} scattering around the base of the Bragg peaks can be attributed to Huang scattering from the static distortions.

In x-ray scattering, the high energy of the x-ray leads to a fast "transit time" so that the structure is effectively frozen. The x-ray scattering is an average over all such frozen structures, which means that the diffraction spectrum is an integral over all frequencies. The quantity W is replaced by $W+W_T+W_F$, where W_T is the thermal part discussed in the previous paragraph and W_F is the contribution from the atomic form factor. The Bragg scattering is still modified by the Debye-Waller factor. The term involving $\langle(\mathbf{Q}\cdot\mathbf{u}_i^T)(\mathbf{Q}\cdot\mathbf{u}_j^T)\rangle_T$ from applying the approximation (14) to the thermal part of (18), leads to thermal diffuse scattering, the divergent piece of which has the form[13]

$$\exp(-2W)\langle(\mathbf{Q}\cdot\mathbf{u}_q^T)(\mathbf{Q}\cdot\mathbf{u}_{-q}^T)\rangle_T=-\exp(-2W)\frac{\hbar}{\pi}\int_{-\infty}^{\infty}\mathrm{Im}[\mathbf{Q}\cdot\overleftrightarrow{G}(q,\omega)\cdot\mathbf{Q}]/[1-\exp(-\hbar\omega/k_BT)]d\omega \ . \tag{22}$$

At zero temperature (22) diverges like q^{-1} around the Bragg peaks and is generally expected to be weak and masked by the Huang scattering. At high temperatures (compared to the Debye temperature), the thermal diffuse scattering (22) becomes

$$-\exp(-2W)k_BT\mathbf{Q}\cdot\overleftrightarrow{G}(\omega=0,q)\cdot\mathbf{Q}/M \ . \tag{23}$$

This has the same form as the divergent part of (15) with the two Green functions being identical except for a factor M, so that the thermal diffuse scattering is like the Huang scattering shown in Fig. 3, including the background terms. The condition that the divergent q^{-2} thermal diffuse scattering is greater than the Huang scattering is again (21). Note that the q^{-2} divergence is obtained at any finite temperature and the q^{-1} divergence is only for strictly zero temperature.

VI. CONCLUSIONS

We have shown that the elastic scattering from a model alloy consists of two parts: the Bragg scattering and the Huang scattering. The Bragg scattering is modulated by a Debye-Waller factor and the divergent Huang scattering comes entirely from the second-order displacement-displacement correlations. Our central approximation (14) has been shown to be essentially numerically exact, and can be used with confidence in more complex alloys and geometries.

ACKNOWLEDGMENTS

We should like to thank E. J. Garboczi, S. D. Mahanti, and S. C. Moss for useful discussions. This work was supported by the National Science Foundation (NSF) under Grant No. DMR 87-14865.

*Permanent address: Department of Physics, Chungbuk National University, Gaeshin-dong, Cheongju-shi, Chungbuk, 360-763, Seoul, Korea.

[1]K. Huang, Proc. R. Soc. London, Ser. A **190**, 102 (1947).

[2]M. F. Thorpe and E. J. Garboczi, Phys. Rev. B **42**, 8405 (1990).

[3]See, for example, R. M. White and T. H. Gabelle, *Solid State Physics* (Academic, New York, 1979), Vol. 15, p. 45.

[4]W. H. Press, B. P. Flannery, S. A. Teukolsky, and W. T. Vetterling, *Numerical Recipes* (Cambridge University, Cambridge, England, 1986), p. 301.

[5]See, for example, N. W. Mermin and N. D. Ashcroft, *Solid State Physics* (Saunders College, Philadelphia, 1976), p. 790.

[6]The most important result from the statistical averaging that we use in this paper is

$$\langle u_{i\alpha}u_{j\beta}\rangle = -Kx(1-x)(L_B^0 - L_A^0)^2 G_{ij}^{\alpha\beta}.$$

The Green function for the fcc lattice is defined as the inverse of the dynamical matrix and is given in E. J. Garboczi and M. F. Thorpe, Phys. Rev. B **32**, 4513 (1985).

[7]L. von Heimendahl and M. F. Thorpe, J. Phys. F **5**, L87 (1975). The masses of the atoms are irrelevant for statics and we set them equal to unity.

[8]M. A. Krivoglaz, *The Theory of X-Ray and Thermal Neutron Scattering from Real Crystals* (Plenum, New York, 1969).

[9]H. E. Cook, J. Phys. Chem. Solids **30**, 1097 (1969); W. Fenzl and S. C. Moss, J. Phys. F **17**, 1285 (1986), and references contained therein.

[10]A. J. C. Wilson, Nature **150**, 152 (1942).

[11]A. A. Maradudin and A. E. Fine, Phys. Rev. **128**, 2589 (1962).

[12]Using the result in I for the total strain energy, it can be shown that the ratio

$$3\langle(\mathbf{u}_i\cdot\hat{\mathbf{R}}_{ij})(\mathbf{u}_j\cdot\hat{\mathbf{R}}_{ij})\rangle/\langle u^2\rangle = 1-\tfrac{1}{2}(1-a^*)/\langle K/\omega^2\rangle = 0.40$$

for the fcc lattice where $a^*=\frac{1}{2}$. These ratios are independent of the concentration x and the length mismatch parameter $(L_B^0-L_A^0)/\bar{L}$.

[13]The required thermal averages are given by

$$\langle u_{i\alpha}^T u_{j\beta}\rangle_T = -(\hbar/\pi)\int_{-\infty}^{\infty} \mathrm{Im}G_{ij}^{\alpha\beta}(\omega)/[1-\exp(-\hbar\omega/k_BT)]d\omega\ ,$$

as discussed, for example, by M. F. Thorpe, Phys. Rev. B **8**, 5352 (1973).